ADVANCED FUNCTIONAL MATERIALS
www.afm-journal.de

Mechanically Rupturing Liquid Metal Oxide Induces Electrochemical Energy

*Xing Ye, Zhaoyi Zheng, Jörg G. Werner, and John William Boley**

Liquid metals, such as Gallium-based alloys, have unique mechanical and electrical properties because they behave like liquid at room temperature. These properties make liquid metals favorable for soft electronics and stretchable conductors. In addition, these metals spontaneously form a thin oxide layer on their surface. Applications made possible by this delicate oxide skin include shape reconfigurable electronics, 3D-printed structures, and unconventional actuators. This paper introduces a new approach where liquid metal oxide serves as an electrochemical energy source. By mechanically rupturing their surface oxide, liquid metals form a galvanic cell and convert their chemical energy to electrical energy. When dispersing liquid metals into an ionically-conductive liquid to form emulsions, this composite material can provide ~500 mV of open-circuit voltage and up to ~4 μW of power. Protected by the naturally occurring oxide skin, the passivating oxide layer of the liquid metal shields it from self-discharge over time. The device is also stable in harsh environments, such as high temperature or aquatic conditions. Future applications of this device are demonstrated by designing a strain-activated stretchable battery and a pressure-sensitive self-powered keypad. These findings may unlock new pathways to design stretchable batteries and harness their inherent energy for self-powered robust devices.

1. Introduction

Liquid metals, such as alloys of gallium, exhibit melting points below room temperature. Unlike mercury, which evaporates and produces toxic vapor, gallium-based liquid metals have practically zero vapor pressure[1,2] and are safe to handle in various applications.[3] They have unique mechanical and electrical properties because they simultaneously behave like a metal and a liquid. These properties make liquid metals an ideal candidate for soft electronics and stretchable conductors. Liquid metals can find their applications in soft electronic circuits,[4–6] stretchable electrical interconnects,[7,8] flexible sensors,[9–11] reconfigurable antennas,[12–14] drug delivery,[15] and hermetic seals.[16] They can also help address current limitations in developing soft and deformable energy solutions for robotic perception,[17] self-sensing,[18] and human-machine interface applications.[19] Liquid metal is also an excellent electrode material for stretchable batteries because it has good deformability and high efficiency owing to its liquid form.[20] A few emerging battery designs featuring gallium-based liquid metals demonstrated promising performance.[21,22] Most of the current designs of liquid metal batteries operate by stripping and depositing metal anodes in alkaline electrolytes.[23] Few gallium-based liquid metal batteries can work in more eco-friendly electrolytes, such as ionic liquid or pH-neutral aqueous solutions.[24]

Despite having many exciting properties, a drawback of gallium-based liquid metals is that they rapidly form a thin layer of oxide on its surface in the presence of oxygen. Until recently, this oxide layer is considered a nuisance because it sticks to many surfaces and interferes with electrochemical measurements.[25] Some applications have turned it into an advantage by exploiting the presence of oxide skin, including manipulating the shape of liquid metals,[26] 3D and 4D printing,[14,27–29] or making unconventional actuators.[30–32] While electrical power generation from thermal oxide nanolayers of iron, vanadium, or nickel has been reported,[33] energy conversion from liquid metal oxide received little attention. As such, the surface oxide could present new opportunities to explore additional interesting properties of liquid metals.

Here, we present a new method of manipulating liquid metal oxide by using it as an electrochemical energy source. Because the formation of liquid metal oxide is a spontaneous process, we seek to harness its electrochemical energy and build a galvanic cell. By mechanically rupturing their surface oxide, liquid metals can form a battery and convert their chemical energy to electrical energy. We introduce a simple composite material with dispersed liquid metal droplets in an ionically-conductive liquid that allows easy device fabrication and customization. The power output of this device is activated by input strain and therefore does not have current leakage at rest, unlike conventional stretchable

X. Ye, J. G. Werner, J. W. Boley
Department of Mechanical Engineering
Boston University
Boston, MA 02215, USA
E-mail: jwboley@bu.edu
Z. Zheng, J. G. Werner, J. W. Boley
Division of Materials Science and Engineering
Boston University
Boston, MA 02215, USA

The ORCID identification number(s) for the author(s) of this article can be found under https://doi.org/10.1002/adfm.202309177

DOI: 10.1002/adfm.202309177

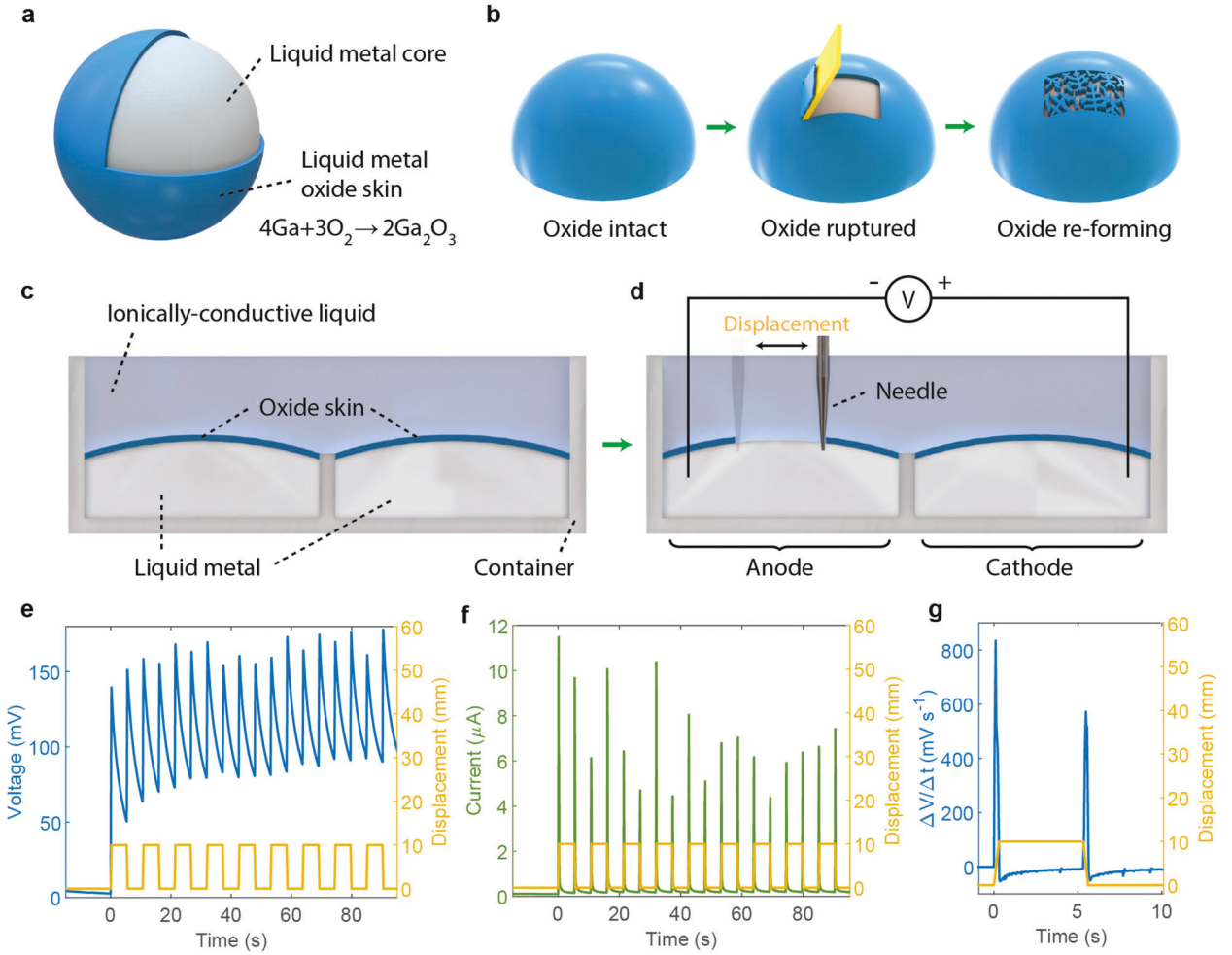

Figure 1. Rupturing liquid metal oxide converts chemical energy to electrical energy. a) The surface of liquid metal is covered by a layer of oxide skin because gallium reacts with oxygen in the environment. b) The liquid metal oxide skin is brittle and can be fractured by mechanical forces, but it quickly re-forms to protect the exposed liquid metal core. c,d) Experimental setup of scratching liquid metal surface with a needle. c) Liquid metal droplets were injected into two separate chambers in a custom container and were immersed in an ionically-conductive liquid electrolyte. d) A needle repeatedly scratched the surface of the liquid metal in one of the chambers to break its oxide skin. The chemical energy of its re-oxidation reaction is partially converted to electrical energy. e) Open-circuit voltage of the system. f) Short-circuit current of the system. g) Derivative of voltage with respect to time during one scratching cycle.

batteries whose chemical reactions occur regardless of their mechanical state. The oxide layer protects the liquid metal from self-discharge over time or changes in ambient conditions, such as high temperature or aquatic environments, which is an advantage over traditional batteries that suffer from stability issues.[34] We demonstrate a strain-activated stretchable battery design that produces ~500 mV of open-circuit voltage and up to ~4 μW of power. This technology could be used in fabricating stretchable batteries with long shelf life and self-powered devices with robust performance.

2. Results

2.1. Scratching Liquid Metal Surface Induces Electrochemical Energy

The liquid metal featured in this study is eutectic gallium-indium (eGaIn). It spontaneously develops a thin and protective oxide layer on its surface in the presence of oxygen (**Figure 1**a).[25,35] This oxide skin is predominantly composed of gallium oxide because gallium oxidation happens more readily than indium.[36,37] Although the oxide skin protects the liquid metal core from further oxidation,[38] this oxide shell itself is brittle and susceptible to mechanical fracture.[39] If the oxide is ruptured in an oxygen-containing environment by mechanical forces, such as stirring or vibration,[40] the oxide skin will rapidly re-form over the liquid metal exposed by the fracture (Figure 1b).[41]

We designed a galvanic cell to harness the electrochemical energy produced by the re-formation of liquid metal oxide skin (Figure 1c). Two drops of bulk liquid metals were injected into a container with two chambers, separated by a solid wall. Oxide skins naturally formed on the surface of the liquid metals during the injection process. Although the liquid metals in the two chambers were not in direct contact with each other, they were both immersed in an ionically-conductive liquid. The ions in this liquid are free to migrate across the liquid electrolyte and

help maintain electrical neutrality.[42] We first used an ionic liquid (1-ethyl-3-methylimidazolium dicyanamide, a salt in liquid form with melting point at -7 °C[43]) for this purpose.

Initially, there was no potential difference between the bulk liquid metal drops in the two sides because they were symmetric (Figure 1d,e, time <0 s). Then, the oxide skin of the liquid metal in the left chamber was mechanically ruptured by puncturing and scratching its surface with a needle, exposing the liquid metal core (Movie S1, Supporting Information). This process disrupted the equilibrium state, and the different interfacial compositions of the two chambers created a galvanic cell. Because the bare liquid metal is energetically unstable and strives towards oxidation to regenerate its oxide skin, the chemical energy of the growth of liquid metal oxide was partially converted into electrical energy, causing a sudden spike in open-circuit voltage or short-circuit current (Figure 1e,f). The voltage or current gradually decreased as fresh oxide layer continued to cover the bare liquid metal. Since moving the needle in the reverse direction also ruptures the oxide skin, we observed similar voltage and current peaks as the needle travelled back to the initial state. At the beginning of a scratching cycle, the open-circuit voltage curve jumped to its peak value simultaneously with the motion of the needle as the oxide skin was ruptured (Figure 1g). The voltage change was fast owing to the short time scale to mechanically fracture of oxide layer (typically within 10^{-3} s of needle movement[44,45]).

On the anode side (left chamber), the bare liquid metal is oxidized[30,46]:

$$2Ga + 3H_2O \rightarrow Ga_2O_3 + 6H^+ + 6e^- \quad (1)$$

Given that Ga_2O_3 is more stable than dissolved gallium ions (such as Ga^{3+}, GaO^+, GaO_2^-) in pH-neutral electrolytes for the gallium-water system,[47] Equation (1) is the only feasible oxidation reaction. Unlike current metal-air batteries in alkaline solutions where the oxidation reaction produces dissolved metal ions,[21,22] here the liquid metal develops new solid oxide skin at the anode.

On the cathode side (right chamber), the dissolved oxygen and the absorbed water in the ionic liquid can be reduced[46,48–50]:

$$O_2 + 2H_2O + 4e^- \rightarrow 4OH^- \quad (2)$$

$$2H_2O + 2e^- \rightarrow H_2 + 2OH^- \quad (3)$$

The reduction of oxygen and water are both thermodynamically possible and happen spontaneously.[49] Equations (2) and (3) are probably happening at the same time, with a relative weight that likely depends on the electrolytes and their respective oxygen and water concentrations.

We can replace ionic liquids with aqueous solutions of salts as the ionically-conductive liquid electrolyte. As an example, a sodium chloride (NaCl) solution was also effective in producing electrical energy (Figures S1 and S2, Supporting Information). It has higher current than that of ionic liquid because of the increased electrical conductivity.[51] To confirm that the presence of liquid metal oxide skin was vital, we conducted a comparison experiment in which sodium hydroxide (NaOH, pH = 14.3) was added to the sodium chloride solution. NaOH, as well as other basic (pH >11) and acidic (pH <3) solutions, etches away the liquid metal oxide.[47] In this case, scratching the surface of liquid metal did not induce voltage or current changes, indicating that rupturing and re-forming oxide skin was essential.

The output voltage depends on a number of factors in the system. On the anode side, the measured potential may be reduced because 1) The exposed liquid metal may react with dissolved oxygen directly instead of releasing energy through the galvanic cell; 2) The growth of oxide skin physically isolates the reactants and prevents further oxidation; 3) The newly formed liquid metal oxide is about two orders of magnitude less conductive than the liquid metal,[40,52] which effectively serves as an electrical barrier. As an example, the concentration of dissolved oxygen in the electrolyte determines the re-growth rate of the oxide skin and hence the voltage decay speed (Figure S3, Supporting Information). On the cathode side, it is also possible to introduce a bias potential to the open circuit voltage by replacing the liquid metal on the cathode side with other materials (Table S1 and Figure S4, Supporting Information).

Because the melting point of the liquid metal alloy increases when its gallium concentration decreases,[53] we expect that the electrochemical reaction eventually stops when the liquid metal solidifies as its melting point increases above room temperature. Our calculations estimate that the reaction can last up to 49 minutes for high current (1 A) applications, and up to 8 years for low current (11.5 μA) applications before the liquid metal solidifies (Experimental Section).

2.2. Liquid Metal-Ionic Liquid Emulsion

Next, we sought to design a viscoelastic material based on the same working principle because it is easier to process and be incorporated in functional devices.[54] We created a composite material consisting of liquid metal and ionic liquid, stabilized by fumed silica nanoparticles (a rheological modifier) to form a emulsion (Experimental Section; Figure S5, Supporting Information). The liquid metal droplets are densely dispersed in a continuous ionic liquid phase instead of settling because the droplets are trapped in kinetically arrested assemblies with fumed silica particles (**Figure 2**a,b).[55,56] These small liquid metal droplets (12.3 μm of average diameter, Figure S6c, Supporting Information) created an abundance of surface to develop oxide skin.

We designed a container filled with this emulsion and inserted two tinned copper wires in parallel passing through it (Figure 2c). The anode wire was pulled and pushed through holes in the container, while the cathode wire remained stationary. When the anode wire was moving inside the emulsion, the wire collided with liquid metal droplets in its path, ruptured their oxide skins temporarily, and thus induced a potential difference (Figure 2d). The liquid metal droplets quickly re-formed their oxide shells, allowing this energy generation process to repeat. Here, the wire acted as a conductive electrode as well as a mechanical agitator. The anode wire itself did not chemically participate in the reaction because the standard reduction potentials of the oxidation of tin and copper (-0.104 V and 0.570 V vs standard hydrogen electrode (SHE), respectively) are higher than that of gallium (-0.485 V vs SHE).[47]

The open-circuit voltage and short-circuit current curves showed similar patterns compared to the results in scratching

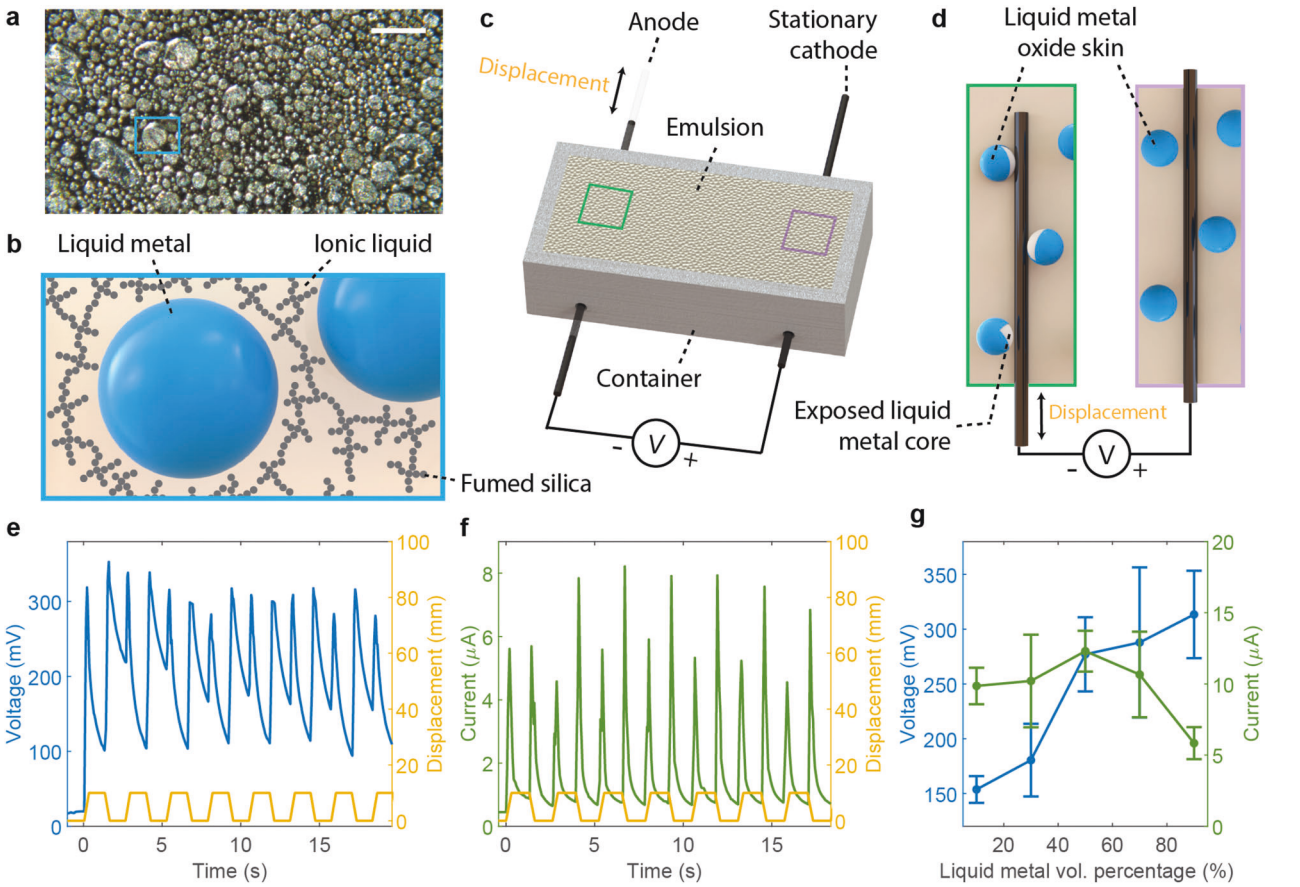

Figure 2. Liquid metal-ionic liquid emulsion. a) Microscope image of emulsion with 90 vol.% of liquid metal. Scale bar represents 100 μm. b) Liquid metal droplets are dispersed in ionic liquid phase and stabilized by fumed silica. c) Relative movement of a rigid wire inside the emulsion induces electrochemcial energy. d) Moving a wire inside the emulsion collides with liquid metal droplets and ruptures their oxide skins. e) Open-circuit voltage of the system. f) Short-circuit current of the system. g) Comparison of peak open-circuit voltage and peak short-circuit current of systems with varying concentrations of liquid metals. Error bars represent standard deviations of three samples.

the surface of bulk liquid metals (Figure 2e,f; Figure S7, Supporting Information). The peak voltage here was higher than that of Figure 1e, likely because the anode wire ruptured more surfaces of liquid metal droplets and the cathode wire was also in contact with the electrolyte. We adjusted the volume percentage of liquid metal in the emulsions and observed that open-circuit voltages increased in emulsions with more liquid metals (Figure 2g). This behavior is because the voltage curves of emulsions with high liquid metal concentrations (i.e., high surface area) and less ionic liquid had long decay time constants, indicating that the regrowth of liquid metal oxide was slower due to the lower amount of oxygen available, and therefore it needed more time to reach a new equilibrium (Figure S8, Supporting Information). The short-circuit current decreased as the emulsion consisted of more liquid metal and less ionic liquid, which limited the availability of oxygen and water.

2.3. Stretchable Strain-Activated Liquid Metal Battery

Based on the working principle of using wires to rupture the oxide skin of liquid metal droplets, we fabricated a series of stretchable devices that can be activated by mechanical strain (Experimental Section; Figure S9, Supporting Information). We used a soft silicone rubber (Ecoflex 00-30) to fully enclose the liquid metal-ionic liquid emulsion (**Figure 3**a). We chose an emulsion with 90 vol.% of liquid metal here because it induced higher voltage than emulsions with other concentrations (Figure 2g). Two wires were embedded in the emulsion as anode and cathode. The anode was formed in a serpentine shape to maximize its contact area with the emulsion and increase collisions with liquid metal droplets, thereby maximizing the peak potential difference. The flexible silicone rubber packaging and the viscoelastic emulsion allowed the device to be stretched reversibly. Because the wire material was stiffer than the emulsion, the anode underwent a translational movement inside the emulsion when the device was stretched and the wire ruptured the oxide skin of collided liquid metal droplets. Similar to the mechanism in the previous section, this process induced a potential difference between the anode and the cathode (Figure 3b,c). When the strain was released, the relative motion of the anode created another spike in open-circuit voltage or short-circuit current. Notably, the peak current was higher when the strain was removed compared to when the device was stretched, likely because of the

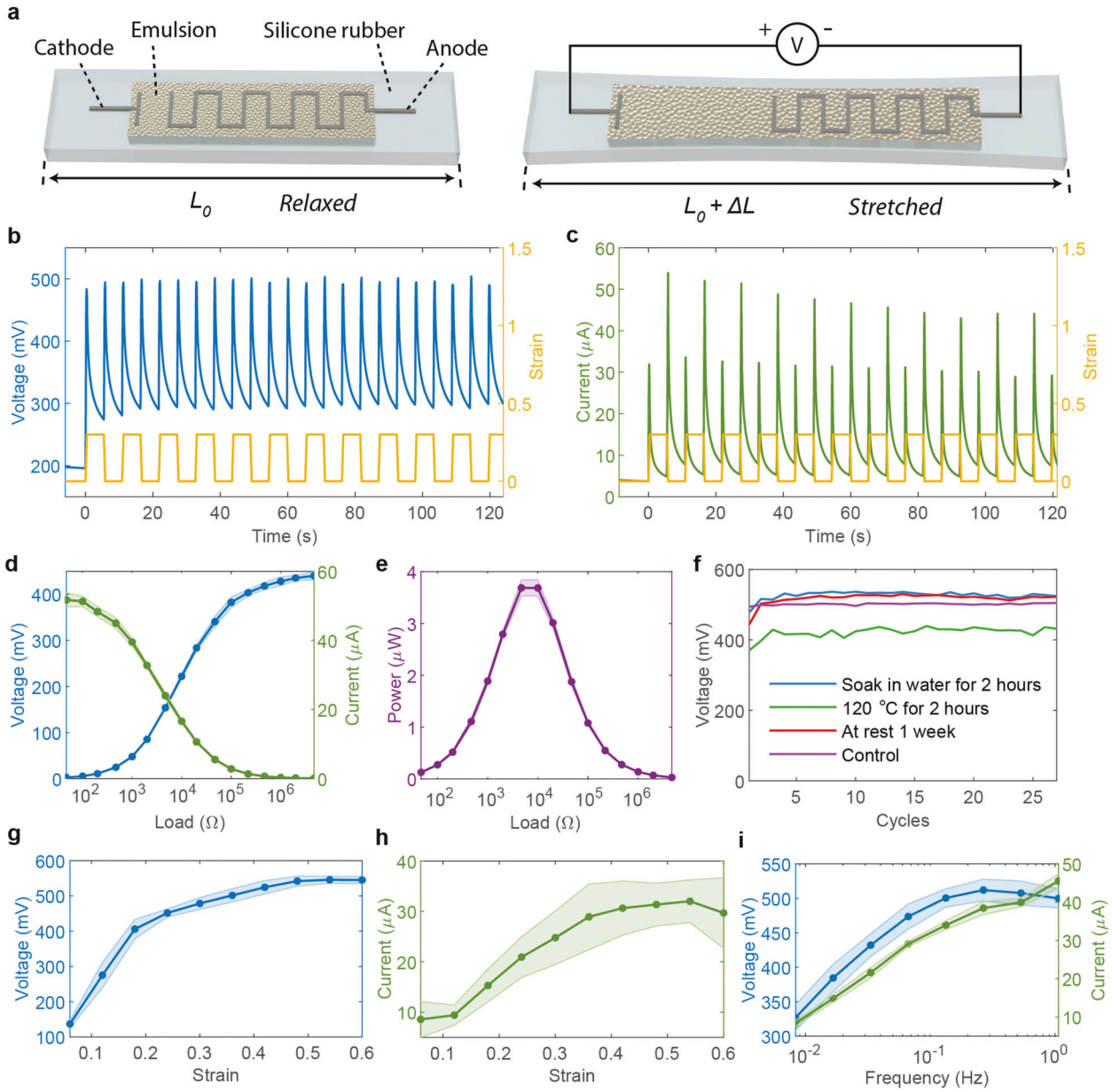

Figure 3. Soft stretchable device featuring liquid metal emulsion with 90 vol.% of liquid metal. a) The device includes rigid wires embedded in the emulsion and is packaged by silicone rubber. Stretching the device causes a relative movement of the anode in the emulsion. Strain is defined as $\Delta L/L_0$. b) Open-circuit voltage of the device. c) Short-circuit current of the device. d) Peak voltage and current of the device under different external loads and strain of 0.3 at 1.3 Hz. Shaded areas represent standard deviations of 20 cycles. e) Peak power of the device under different external loads and strain of 0.3 at 1.3 Hz. Shaded areas represent standard deviations of 20 cycles. f) Peak voltages of four devices under strain of 0.3 at 0.1 Hz in different ambient conditions. The at-rest sample was fabricated one week before testing. The underwater sample was immersed in deionized water for 2 hours and dried in ambient environment before testing. The high-temperature sample was heated to 120 °C for 2 h and then tested after it was cooled to room temperature. The control group was tested the same day of manufacture in ambient environment (21.2 °C, 51.1% relative humidity). g) Peak voltages under different strain inputs at 0.1 Hz. Shaded areas represent standard deviations of ten cycles. h) Peak currents under different strain inputs at 0.1 Hz. Shaded areas represent standard deviations of ten cycles. i) Peak voltages and currents at various stretching frequencies under strain of 0.3. Shaded areas represent standard deviations of five cycles.

shorter distance between the two electrodes in the relaxed state (Figure 3c).[57,58]

The electrical output performance of this device depended on its external load. With higher load resistance, the peak voltage increased, while the peak current decreased (Figure 3d). The maximum peak power was ~4 μW under an optimal load of 4.7 kΩ (Figure 3e). The instantaneous power density (normalized by the surface area of the cathode) was 35.6 mWm^{-2}, which was higher than that of electrical-double-layer (0.5 mWm^{-2}).[59] or piezoelectric energy harvesters (1.2 μWm^{-2}),[60] and similar to triboelectric

nanogenerators (35 mWm^{-2}).[61] In addition, stretching the device at higher frequencies and under higher strains can improve its output performance, likely because the increased collisions between the anode and liquid metal droplets created more oxide ruptures (Figure 3g–i). The device can be stretched to uniaxial tensile strain of up to 1.9 reversibly without negatively affecting its output performance (Figure S10, Supporting Information).

We also investigated the cycling, at-rest, thermal, and aquatic stability of these batteries. A device was stretched and released continuously for 20 000 cycles at 0.5 Hz to test its fatigue behavior (Figure S11, Supporting Information). We observed that the liquid metal droplets started to coalesce as the collision between the electrode and droplets continued. The peak voltage slightly decreased from ~650 mV as the liquid metal droplets coalesced and liquid metal oxide fragments accumulated. The voltage maintained ~500 mV when coalescence appeared to stop. Because the oxide skin shielded the liquid metal inner core from external environment, the devices also performed well even after being subject to ambient conditions that are typically harsh for batteries, such as high temperature or aquatic environments (Figure 3f). The sample in high temperature exhibited slightly lower voltage than other samples, possibly because the evaporation of water in the sample limited its electrochemical reaction. Due to the protection provided by the passivating oxide skin and zero vapor pressure of the ionic liquid, the device remained shelf-stable after being manufactured without self-discharge, as demonstrated by a sample resting in ambient environment for seven days (Figure 3f). These results demonstrated good stability of these stretchable batteries.

2.4. Applications of Liquid Metal Emulsion-Based Devices

Despite the peak voltage output of the liquid metal battery is limited to ~500 mV, it is possible to increase the voltage by connecting multiple devices in series. As an example, we combined eight devices to boost the output voltage (**Figure 4**a). Here, the emulsion in each device was constrained in their individual chamber and separated by silicone rubber, but the anode of one chamber was electrically connected to the cathode in the next chamber. The induced energy of this composite device was sufficient to power an LED (light emitting diode) when the soft battery was stretched (Figure 4b,c; Movie S2, Supporting Information).

We can also use this type of liquid metal emulsion-based device as a sensor without external power because it intrinsically responds to mechanical changes. We fabricated a soft self-powered keypad that produced voltage changes when the buttons were compressed (Figure 4d,e). The embedded rigid anodes deflected and ruptured the liquid metal oxide in the emulsion, causing a sudden change in voltage output. A microcontroller registered these transient voltage changes and sent signals to a computer, which displayed the corresponding characters (Figure 4f; Figure S12 and Movie S3, Supporting Information). The simplicity of this self-powered sensor design allows scalability and easy integration with other electronic components.

3. Conclusions, Limitations, and Future Work

We presented a method to induce electrochemical energy conversion from liquid metal by rupturing its outer oxide skin. The chemical energy of the spontaneous re-formation of the liquid metal oxide layer converts to electrical energy and it can be used as a new type of soft battery. Based on this technique, we demonstrated a stretchable battery design featuring an emulsion composed of liquid metal and ionic liquid. This simple structure was capable of producing up to ~500 mV and 3.5 μW of power when stretched. Protected by the liquid metal oxide skin, the device has great stability and performs well in a variety of harsh environments. The battery delivers power on demand and remains dormant at rest. It can power other electronic components and can also serve as a self-powered mechanically-activated sensor. The device design is general, customizable, and easy to implement. Other manufacturing techniques may also be used for achieving scalability, such as 3D printing,[28] lithography,[62] continuous flow sonication,[63] and parallelization of emulsion production.[64] These features make it a desirable candidate for soft and stretchable energy devices. This technology is also particularly suitable for other low-power applications, such as strain-activated electronic switches, vibration-sensitive detection systems, and hibernating devices that can be woken up by external mechanical events.

It is possible to further improve the output energy of this type of system. For example, there are other metal elements that develop oxide layers more easily than gallium according to the standard Gibbs free energy of formation of their corresponding oxides (Figure S13, Supporting Information).[47,65] We can increase the open-circuit voltage of the electrochemical cell by doping gallium-indium liquid metal with metal elements that have lower standard reduction potentials and may form oxide preferentially over gallium. One of the potential candidates is aluminum. Aluminum-doped liquid metal can produce 1.951 V of maximum voltage in theory,[47,66] which is promising as a stretchable battery or self-powered sensor for many future applications. Some rare-earth elements can also produce higher voltage, but their applications may be limited due to supply shortage and high cost.

We note that the output current was not optimized in this study and it could be improved by adjusting the conductivity of the liquid metal emulsion. For example, metal-containing ionic liquids are highly conductive electrolytes with increased current densities.[67] Polymeric ionic liquid electrolytes also exhibited high ion-conductive properties in battery systems.[68,69] In addition, because copper wires are susceptible to corrosion when exposed to liquids,[70] other materials for the wires could be more suitable to avoid any potential long-term corrosion. Future investigations may also involve exploring other electrolytes (organic solvents and potential impurities in ionic liquids) and implementing strategies to make this device rechargeable, such as ionic liquid-based electrolysis.[71,72] Altogether, this technology may inspire new battery designs featuring liquid metal surface oxide and open up new opportunities to harness their inherent energy for self-powered soft devices.

4. Experimental Section

Materials: Liquid metal (Metspec 60, 5N Plus), ionic liquid (1-ethyl-3-methylimidazolium dicyanamide, Basionics VS 03, ⩾ 98%, BASF SE), sodium chloride (99+%, Acros Organics), sodium hydroxide (⩾ 98%,

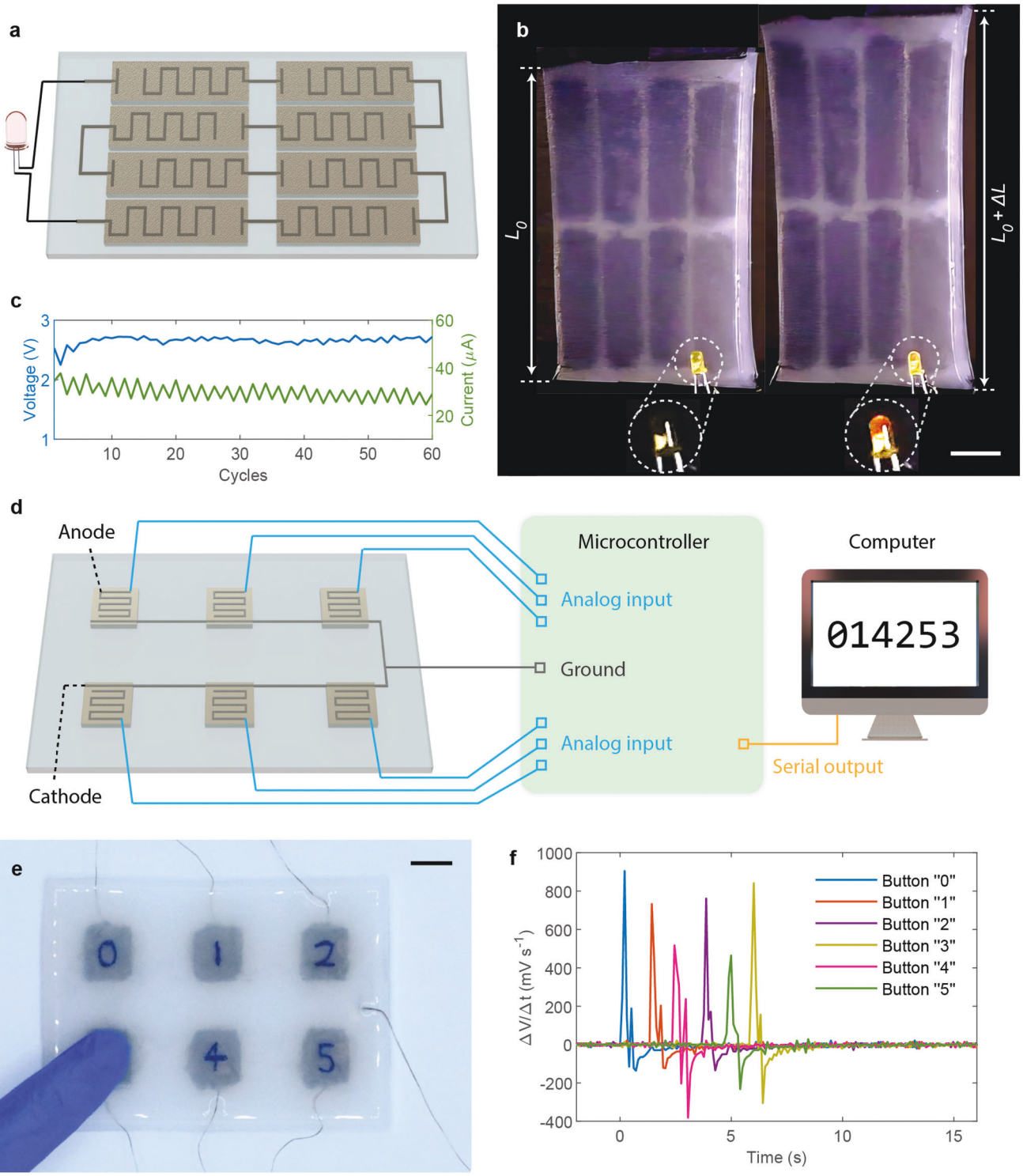

Figure 4. Applications of the liquid metal emulsion-based device. a) A liquid metal battery comprised of multiple interconnected devices. b) The stretchable battery was capable of powering a LED. The circular inset images showed the same LED in a darker environment. Scale bar represents 10 mm. c) Peak voltage and current of the device under strain of 0.3 at 0.5 Hz. d) A soft keypad that responds to compression without external power. A microcontroller processes the voltage signal and sends it to the computer for display. e) The compression-responsive keypad reacts to mechanical inputs by a finger. Scale bar represents 10 mm. f) Derivative of voltage with respect to time of the six buttons of the keypad when they were pressed.

Sigma–Aldrich), fumed silica (Aerosil R 104, Evonik), and Ecoflex (00-30, Smooth-On) were used as received.

Scratching Liquid Metal Surface: A plastic needle (SmoothFlow Tapered Precision Dispense Tip, Gauge 27, Nordson) was secured on a linear stage (ATS150, Aerotech) of a custom gantry system (Aerotech). The controller of the gantry system (A3200, Aerotech) was programmed to move the needle at a velocity of 40 mms^{-1}. The timestamps of the beginning and the end of the movement of the needle were recorded for the displacement curves. Liquid metals were injected into a 3D-printed container (Form 3+, Formlabs) with two chambers. Ionic liquid was poured into the container and fully covered the surfaces of liquid metals. A digital multimeter (34465A, Keysight) was used to record the voltage or current between the liquid metals in the two chambers through tinned copper wires. The wires were electrically insulated from the liquid electrolyte and were in contact with liquid metals only. The electrochemical measurements were performed on a potentiostat/galvanostat (Interface 1010E, Gamry Instruments).

Estimation of Reaction Lifetime of Forming Gallium Oxide: The melting point of eGaIn changed depending on its composition. It transitions from 15.7 °C (below room temperature, 24 wt.% of indium) to 22.2 °C (room temperature, 28.7 wt.% of indium).[53] The mass of EGaIn in a chamber of the container was 3.69 g. The liquid metal will not solidify until 0.71 g, or 0.0102 mol, of gallium is consumed. This process will transfer 0.0306 mol of electrons, which is equivalent to a theoretic capacity of 222.3 $mAh \cdot g^{-1}$. Based on the maximum output current (11.5 μA, Figure 1f), the process of formation of gallium oxide can last at least 2.6×10^8 s (8 years). At 1 A, a typical discharge current of alkaline batteries,[73] the reaction can last 2.9×10^3 s (49 min).

Preparation of Liquid Metal-Ionic Liquid Emulsions: Liquid metal and ionic liquid were weighed into a 20 mL capacity plastic cup and mixed in a SpeedMixer (DAC 150.1 FVZ-K, FlackTek) at 3500 rpm. Fumed silica was added to this mixture and mixed at 3500 rpm (Figure S3, Supporting Information). See Table S2 (Supporting Information) for details about the masses of each component and mixing time.

Optical Image of Liquid Metal-Ionic Liquid Emulsion: The microscopic image of the liquid metal-ionic liquid emulsion was captured by a camera (U3-30C0CP Rev.2.2, IDS Imaging) with a miniature microscope system (InfiniTube FM-200, Infinity; Achrovid 10x objective, Infinity). The particle size distribution was determined by importing a microscopic image into an image analysing software (ImageJ2), segmenting the image to binary format (Huang thresholding method, Black and white color), and then calculating the diameters of the particles based on elliptical approximation (circularity 0.00–1.00) (Figure S4a,b, Supporting Information).

Pulling Wire Inside Emulsion: The liquid metal-ionic liquid emulsion was transferred to a 3D-printed container (Form 3+). Two tinned copper solid-core wires, stripped of their insulating layers, were inserted in the emulsion through holes in the container. One of the wires was secured on a linear stage (ATS150) of the gantry system. The controller of the gantry system (A3200) was programmed to pull and push the wire at a velocity of 40 mm s^{-1} while a digital multimeter (34465A) was recording voltage or current.

Fabrication of Stretchable Devices: The main part of the silicone rubber packaging was made by pouring a mixture of equal weight of Ecoflex 00-30 Parts A and B into a 3D-printed mold (Form 3+) and then demolded after curing in room temperature for 4 h. The liquid metal-ionic liquid emulsion was then transferred to the center chamber of the silicone rubber packaging. Two tinned copper wires were placed inside the emulsion. Finally, additional mixture of equal weight of Ecoflex 00-30 Parts A and B was poured on the top of the device and allowed curing in room temperature for another 4 h (Figure S6, Supporting Information).

Characterization of Stretchable Devices: The devices were secured on the linear stage (ATS150) of the custom gantry system through a pair of metal clamps and a custom fixture. The controller of the gantry system (A3200) was programmed to stretch and release the devices while a digital multimeter (34465A) was recording their voltages or currents. For tests with different external loads, the output voltages and currents were measured separately. The voltage data was obtained by connecting various resistors in parallel with the measurement device while measuring its voltage (Figure S14a, Supporting Information), and the current data was obtained by connecting various resistors in series with the measurement device while measuring its current (Figure S14b, Supporting Information). The power was calculated by multiplying the respective voltage and current. The stress-strain, stress-voltage, and stress-current curves were obtained by applying uniaxial tensile stress to samples on a single-column mechanical testing system (5944, Instron). The samples were stretched and released at a speed of 40 $mm\ s^{-1}$ while a digital multimeter (34465A) was recording their open-circuit voltages or short-circuit currents.

Characterization of the Keypad: The six buttons of the device shared the same cathode and it was connected the ground pin of a microcontroller (UNO R3, Arduino). The anodes were individually connected to analog input pins through bias resistors. The microcontroller sent voltage data of six analog input channels to a Python program on a computer via serial communication. The computer program detected the voltage changes of the six channels and displayed button inputs on a graphical user interface.

Supporting Information

Supporting Information is available from the Wiley Online Library or from the author.

Acknowledgements

This work was supported by the Air Force Office of Research Young Investigator Award (FA9550-20-1-0365; J.W.B.), the National Science Foundation CAREER Award (CMMI2047683; J.W.B., X.Y.), and the National Science Foundation Award (CBET-2146597; J.G.W.). The authors thank Javier M. Morales Ferrer, Ramón E. Sánchez Cruz, and Stephanie F. Zopf for their technical assistance.

Conflict of Interest

The authors declare no conflict of interest.

Data Availability Statement

The data that support the findings of this study are available in the supplementary material of this article.

Keywords

electrochemical energy, liquid metal emulsions, liquid metal oxides, stretchable batteries

Received: August 4, 2023
Revised: September 28, 2023
Published online:

[1] C. Cochran, L. Foster, *J. Electrochem. Soc.* **1962**, *109*, 144.
[2] N. Morley, J. Burris, L. Cadwallader, M. Nornberg, *Rev. Sci. Instrum.* **2008**, *79*, 5.
[3] J. Chandler, H. Messer, G. Ellender, *J. Dent. Res.* **1994**, *73*, 1554.
[4] J. Ma, F. Krisnadi, M. H. Vong, M. Kong, O. M. Awartani, M. D. Dickey, *Adv. Mater.* **2023**, *35*, 2205196.
[5] A. F. Silva, H. Paisana, T. Fernandes, J. Góis, A. Serra, J. F. Coelho, A. T. de Almeida, C. Majidi, M. Tavakoli, *Adv. Mater. Technol.* **2020**, *5*, 2000343.

[6] T. H. Park, J.-H. Kim, S. Seo, *Adv. Funct. Mater.* **2020**, *30*, 2003694.
[7] J. Yoon, S. Y. Hong, Y. Lim, S.-J. Lee, G. Zi, J. S. Ha, *Adv. Mater.* **2014**, *26*, 6580.
[8] N. Lazarus, C. Meyer, W. Turner, *RSC Adv.* **2015**, *5*, 78695.
[9] G. Yun, S.-Y. Tang, S. Sun, D. Yuan, Q. Zhao, L. Deng, S. Yan, H. Du, M. D. Dickey, W. Li, *Nat. Commun.* **2019**, *10*, 1300.
[10] C. B. Cooper, K. Arutselvan, Y. Liu, D. Armstrong, Y. Lin, M. R. Khan, J. Genzer, M. D. Dickey, *Adv. Funct. Mater.* **2017**, *27*, 1605630.
[11] A. P. Gerratt, H. O. Michaud, S. P. Lacour, *Adv. Funct. Mater.* **2015**, *25*, 2287.
[12] B. Yao, X. Xu, Q. Zhang, H. Yu, H. Li, L. Ren, S. Perini, M. Lanagan, Q. Wang, H. Wang, *Mater. Lett.* **2020**, *270*, 127727.
[13] A. Qusba, A. K. RamRakhyani, J.-H. So, G. J. Hayes, M. D. Dickey, G. Lazzi, *IEEE Sens. J.* **2014**, *14*, 1074.
[14] J. W. Boley, W. M. Van Rees, C. Lissandrello, M. N. Horenstein, R. L. Truby, A. Kotikian, J. A. Lewis, L. Mahadevan, *Proc. Nat. Acad. Sci. U. S. A.* **2019**, *116*, 20856.
[15] V. K. Truong, A. Hayles, R. Bright, T. Q. Luu, M. D. Dickey, K. Kalantar-Zadeh, K. Vasilev, *ACS Nano* **2023**, *17*, 14406.
[16] Q. Shen, M. Jiang, R. Wang, K. Song, M. H. Vong, W. Jung, F. Krisnadi, R. Kan, F. Zheng, B. Fu, P. Tao, C. Song, G. Weng, B. Peng, J. Wang, W. Shang. M. D. Dickey, T. Deng, *CScience* **2023**, *379*, 488.
[17] H. Wang, M. Totaro, L. Beccai, *Adv. Sci.* **2018**, *5*, 1800541.
[18] L. Cao, D. Yu, Z. Xia, H. Wan, C. Liu, T. Yin, Z. He, *Adv. Mater.* **2020**, *32*, 2000827.
[19] Y. Wu, Y. Zhou, W. Asghar, Y. Liu, F. Li, D. Sun, C. Hu, Z. Wu, J. Shang, Z. Yu, R.-W. Li, H. Yang, *Adv. Intell. Syst.* **2021**, *3*, 2000235.
[20] H. Fu, G. Liu, L. Xiong, M. Wang, J. Lee, R. Ren, W. Yang, J. K. Lee, *Adv. Funct. Mater.* **2021**, *31*, 2107062.
[21] G. Liu, J. Y. Kim, M. Wang, J.-Y. Woo, L. Wang, D. Zou, J. K. Lee, *Adv. Energy Mater.* **2018**, *8*, 1703652.
[22] D. Liu, L. Su, J. Liao, B. Reeja-Jayan, C. Majidi, *Adv. Energy Mater.* **2019**, *9*, 1902798.
[23] Z. Xing, J. Fu, S. Chen, J. Gao, R. Zhao, J. Liu, *Front. Energy* **2022**, *16*, 23.
[24] J. Gao, J. Ye, S. Chen, J. Gong, Q. Wang, J. Liu, *ACS Appl. Mater. Interfaces* **2021**, *13*, 17093.
[25] M. D. Dickey, *ACS Appl. Mater. Interfaces* **2014**, *6*, 18369.
[26] M. R. Khan, C. B. Eaker, E. F. Bowden, M. D. Dickey, *Proc. Nat. Acad. Sci. U. S. A.* **2014**, *111*, 14047.
[27] J. W. Boley, E. L. White, G. T.-C. Chiu, R. K. Kramer, *Adv. Funct. Mater.* **2014**, *24*, 3501.
[28] R. E. Sánchez Cruz, S. F. Zopf, J. W. Boley, *J. Compos. Mater.* **2023**, *57*, 829.
[29] R. Xing, J. Yang, D. Zhang, W. Gong, T. V. Neumann, M. Wang, R. Huang, J. Kong, W. Qi, M. D. Dickey, *Matter* **2023**, *6*, 2248.
[30] R. C. Gough, J. H. Dang, M. R. Moorefield, G. B. Zhang, L. H. Hihara, W. A. Shiroma, A. T. Ohta, *ACS Appl. Mater. Interfaces* **2016**, *8*, 6.
[31] R. C. Gough, A. M. Morishita, J. H. Dang, M. R. Moorefield, W. A. Shiroma, A. T. Ohta, *Micro Nano Syst. Lett.* **2015**, *3*, 4.
[32] C. B. Eaker, M. D. Dickey, *Appl. Phys. Rev.* **2016**, *3*, 3.
[33] M. D. Boamah, E. H. Lozier, J. Kim, P. E. Ohno, C. E. Walker, T. F. Miller III, F. M. Geiger, *Proc. Nat. Acad. Sci. U. S. A.* **2019**, *116*, 16210.
[34] B. E. Conway, W. Pell, T. Liu, *J. Power Sources* **1997**, *65*, 53.
[35] Z. Zhao, S. Soni, T. Lee, C. A. Nijhuis, D. Xiang, *Adv. Mater.* **2023**, *35*, 2203391.
[36] R. C. Chiechi, E. A. Weiss, M. D. Dickey, G. M. Whitesides, *Angew. Chem., Int. Ed.* **2008**, *47*, 142.
[37] A. Zavabeti, J. Z. Ou, B. J. Carey, N. Syed, R. Orrell-Trigg, E. L. Mayes, C. Xu, O. Kavehei, A. P. O'Mullane, R. B. Kaner, K. Kalantar-Zadeh, T. Daeneke, *Science* **2017**, *358*, 332.
[38] B. D. Anderson, J. B. Tracy, *Nanoscale* **2014**, *6*, 12195.
[39] M. D. Dickey, R. C. Chiechi, R. J. Larsen, E. A. Weiss, D. A. Weitz, G. M. Whitesides, *Adv. Funct. Mater.* **2008**, *18*, 1097.
[40] D. Wang, X. Wang, W. Rao, *Acc. Mater. Res.* **2021**, *2*, 1093.
[41] J. M. Chabala, *Phys. Rev. B* **1992**, *46*, 11346.
[42] R. Holze, *Experimental Electrochemistry: A Laboratory Textbook*, John Wiley & Sons, New York, USA **2019**.
[43] K. Bernardino, T. A. Lima, M. C. Ribeiro, *J. Phys. Chem. B* **2019**, *123*, 9418.
[44] J. R. Goldberg, J. L. Gilbert, *J. Biomed. Mater. Res* **1997**, *37*, 421.
[45] S. Liu, S. N. Reed, M. J. Higgins, M. S. Titus, R. Kramer-Bottiglio, *Nanoscale* **2019**, *11*, 17615.
[46] J. Wang, F. Tang, Y. Wang, Q. Lu, S. Liu, L. Li, *ACS Appl. Mater. Interfaces* **2019**, *12*, 1558.
[47] M. Pourbaix, *Atlas of Electrochemical Equilibria in Aqueous Solutions*, NACE, Pennsylvania, USA **1966**.
[48] J. A. Widegren, A. Laesecke, J. W. Magee, *Chem. Commun.* **2005**, *2005*, 1610.
[49] M. Jia, J. T. Newberg, *J. Phys. Chem. C* **2019**, *123*, 28688.
[50] Z. Zhou, Z. Xing, Q. Wang, J. Liu, *Small* **2023**, *7*, 2207327.
[51] J. Vila, P. Gines, E. Rilo, O. Cabeza, L. Varela, *Fluid Phase Equilib.* **2006**, *247*, 32.
[52] C. A. Nijhuis, W. F. Reus, G. M. Whitesides, *J. Am. Chem. Soc.* **2009**, *131*, 17814.
[53] J. P. Denny, J. H. Hamilton, J. R. Lewis, *JOM* **1952**, *4*, 39.
[54] T. J. Ober, D. Foresti, J. A. Lewis, *Proc. Nat. Acad. Sci. U. S. A.* **2015**, *112*, 12293.
[55] F. Macedo Fernandes Barros, C. Chassenieux, T. Nicolai, M. M. de Souza Lima, L. Benyahia, *J. Dispersion Sci. Technol.* **2019**, *40*, 1169.
[56] F. Gautier, M. Destribats, R. Perrier-Cornet, J.-F. Dechézelles, J. Giermanska, V. Héroguez, S. Ravaine, F. Leal-Calderon, V. Schmitt, *Phys. Chem. Chem. Phys.* **2007**, *9*, 6455.
[57] A. Susanto, M. S. Baskoro, S. H. Wisudo, M. Riyanto, F. Purwangka, *Int. J. Renew. Energy Res.* **2017**, *7*, 298.
[58] P. Y. Furlan, T. Krupa, H. Naqiv, K. Anderson, *J. Chem. Educ.* **2013**, *90*, 1341.
[59] V. Vallem, E. Roosa, T. Ledinh, W. Jung, T.-i. Kim, S. Rashid-Nadimi, A. Kiani, M. D. Dickey, *Adv. Mater.* **2021**, *33*, 2103142.
[60] Y. Yang, H. Pan, G. Xie, Y. Jiang, C. Chen, Y. Su, Y. Wang, H. Tai, *Sens. Actuators, A* **2020**, *301*, 111789.
[61] X. Pu, M. Liu, X. Chen, J. Sun, C. Du, Y. Zhang, J. Zhai, W. Hu, Z. L. Wang, *Sci. Adv.* **2017**, *3*, e1700015.
[62] Y. Xia, G. M. Whitesides, *Annu. Rev. Mater. Sci.* **1998**, *28*, 153.
[63] S. Kuhn, T. Noël, L. Gu, P. L. Heider, K. F. Jensen, *Lab Chip* **2011**, *11*, 2488.
[64] A. Ofner, D. G. Moore, P. A. Rühs, P. Schwendimann, M. Eggersdorfer, E. Amstad, D. A. Weitz, A. R. Studart, *Macromol. Chem. Phys.* **2017**, *218*, 1600472.
[65] D. R. Lide, *CRC Handbook of Chemistry and Physics*, 85th edition, CRC press, Boca Raton, USA **2004**.
[66] D. W. Ball, *Physical Chemistry*, Cengage Learning, Massachusetts, USA **2011**.
[67] N. R. Brooks, S. Schaltin, K. Van Hecke, L. Van Meervelt, K. Binnemans, J. Fransaer, *Chem.- Eur. J.* **2011**, *17*, 5054.
[68] Y. Tominaga, *Polym. J.* **2017**, *49*, 291.
[69] F. Zhang, Y. Sun, Z. Wang, D. Fu, J. Li, J. Hu, J. Xu, X. Wu, *ACS Appl. Mater. Interfaces* **2020**, *12*, 23774.
[70] M. Uerdingen, C. Treber, M. Balser, G. Schmitt, C. Werner, *Green Chem.* **2005**, *7*, 321.
[71] J. Wang, K. Appusamy, S. Guruswamy, A. Nahata, *Sci. Rep.* **2015**, *5*, 8637.
[72] J. Wu, P. Xie, W. Hao, D. Lu, Y. Qi, Y. Mi, *Front. Chem.* **2022**, *10*, 1014893.
[73] G. V. Riley, D. S. Hussey, D. Jacobson, *ECS Trans.* **2010**, *25*, 75.